

The Evolution of Dark Canopies Around Active Regions

Y.-M. Wang

*Code 7672W, Space Science Division, Naval Research Laboratory, Washington, DC
20375-5352, USA*

`yi.wang@nrl.navy.mil`

E. Robbrecht

Royal Observatory of Belgium, 1180 Brussels, Belgium

`eva.robbrecht@oma.be`

and

K. Muglach¹

Code 674, NASA Goddard Space Flight Center, Greenbelt, MD 20771, USA

`karin.muglach@nasa.gov`

ABSTRACT

As observed in spectral lines originating from the chromosphere, transition region, and low corona, active regions are surrounded by an extensive “circumfacular” area which is darker than the quiet Sun. We examine the properties of these dark moat- or canopy-like areas using Fe IX 17.1 nm images and line-of-sight magnetograms from the *Solar Dynamics Observatory*. The 17.1 nm canopies consist of fibrils (horizontal fields containing EUV-absorbing chromospheric material) clumped into featherlike structures. The dark fibrils initially form a quasiradial or vortical pattern as the low-lying field lines fanning out from the emerging active region connect to surrounding network and intranetwork elements of the opposite polarity. The area occupied by the 17.1 nm fibrils expands as supergranular convection causes the active region flux to spread into the background medium; the outer boundary of the dark canopy stabilizes where the diffusing flux encounters a unipolar region of the opposite sign. The dark fibrils tend to accumulate in regions of weak longitudinal field and to become rooted in mixed-polarity flux. To

¹Also at ARTEP, Inc., Ellicott City, MD 21042, USA.

explain the latter observation, we note that the low-lying fibrils are more likely to interact with small loops associated with weak, opposite-polarity flux elements in close proximity, than with high loops anchored inside strong unipolar network flux. As a result, the 17.1 nm fibrils gradually become concentrated around the large-scale polarity inversion lines (PILs), where most of the mixed-polarity flux is located. Systematic flux cancellation, assisted by rotational shearing, removes the field component transverse to the PIL and causes the fibrils to coalesce into long PIL-aligned filaments.

Subject headings: Sun: activity — Sun: corona — Sun: filaments, prominences — Sun: magnetic topology — Sun: surface magnetism — Sun: UV radiation

1. Introduction

Active regions are often surrounded by an area whose brightness is reduced even relative to that of the quiet Sun. This phenomenon was first noted in observations of “circumfacular regions” in the Ca II K-line (Hale & Ellerman 1903; St. John 1911). The dark areas, also prominent in Ca II 854.2 nm spectroheliograms, were subsequently shown to coincide approximately with the iron-filing or “vortex” pattern of H α fibrils that rapidly appears around emerging active regions (Howard & Harvey 1964; Bumba & Howard 1965; Veeder & Zirin 1970; Foukal 1971a, 1971b; Harvey 2005, 2006; Rutten 2007; Cauzzi et al. 2008; Reardon et al. 2009). During the first week of development, the major axis of the fibril pattern expands at a rate of ~ 0.2 km s $^{-1}$, corresponding to roughly one supergranular cell radius per day.

With the advent of UV and extreme-ultraviolet (EUV) observations, it is now evident that the reduced emission around active regions characterizes a wide range of spectral lines originating in the chromosphere, transition region, and low corona (Moses et al. 1997; Feldman et al. 2000). Indeed, in emission lines formed at temperatures $T \sim 0.5$ – 1.0 MK and in He II 30.4 nm, these large moatlike areas, or “active-region canopies” as we henceforth call them, are sometimes mistaken for coronal holes. Like their H α counterparts, the EUV canopies consist of dark fibrillar structures, which are generally thought to trace out horizontal magnetic fields in the chromosphere.

Here, we use Fe IX 17.1 nm images and longitudinal magnetograms recorded with the *Solar Dynamics Observatory* (*SDO*) to study the properties of dark canopies around active regions. Our main objective is to clarify the relationship between the 17.1 nm fibril structures and the evolving photospheric field, on the assumption that the fibrils are aligned with the

chromospheric field. We do not address the question of how the EUV canopies differ from those seen in the visible, or the related and more difficult question of how the spectral lines themselves are formed.

2. Observations

The Atmospheric Imaging Assembly (AIA) on *SDO* records full-disk images in seven EUV, two UV, and one white-light channel, with $0''.6$ pixels and 10 s cadence.¹ The Helioseismic and Magnetic Imager (HMI) provides longitudinal magnetograms with similar spatial resolution, taken every 45 s in Fe I 617.3 nm.² The AIA and HMI images were coaligned using the disk centers as the common reference point, after correcting for the factor of 0.844 plate-scale difference, determined from the ratio of AIA 170.0 nm and HMI disk diameters in pixels. The data employed here are all from the period 2010 August–September, early during the rising phase of solar cycle 24.

As an illustrative example, Figure 1 shows a large, decaying active region (NOAA 11100) in the southern hemisphere, as it appeared at 23:01 UT on 2010 August 20. At the left are AIA images recorded in Fe IX 17.1 nm (characteristic temperature $T \sim 0.7$ MK), He II 30.4 nm, and Fe XIV 21.1 nm ($T \sim 2.0$ MK). At the right are three versions of a simultaneous HMI magnetogram, saturated respectively at ± 100 G, ± 30 G (after smoothing to $2''$ resolution), and ± 0.1 G (after smoothing with a $60'' \times 60''$ running window). From the 17.1 nm image, we see that the active region, which emerged one month earlier and is centered at latitude $L \sim -23^\circ$, is surrounded by a dark area that extends equatorward (poleward) as far as $L \sim -5^\circ$ ($L \sim -50^\circ$). This canopy consists of leaf- or featherlike structures that fan out more or less radially from the active region. The He II 30.4 nm image shows a dark canopy of similar shape and extent; from this correspondence, we conclude that the dark 17.1 nm features are analogous to the He II fibrils and filaments displayed in Wang (2001), which resemble but occupy larger volumes than their well-known $H\alpha$ counterparts. (Unless otherwise noted, the term “fibril” hereinafter refers to features seen in 17.1 nm.) The canopy is much less visible in the Fe XIV 21.1 nm image, being partially obscured by diffuse emission from the overlying coronal loops. Conversely, quiet Sun areas outside the canopy (as at the upper left and upper right corners of the images) are darker in the higher-temperature lines than in 17.1 nm.

¹Daily full-resolution images may be viewed at <http://sdowww.lmsal.com/suntoday>.

²See <http://hmi.stanford.edu>.

Comparing the Fe IX image (Figure 1(a)) with the line-of-sight magnetograms (Figures 1(d) and 1(e)), we see that the dark features in 17.1 nm are generally centered above areas of *relatively* weak photospheric flux, as expected if they trace out horizontal fields. These locations of reduced $|B_r|$ include not only the supergranular cell interiors, but also more extensive areas of mixed polarity, where the spreading active-region flux encounters background regions of the opposite polarity. The boxes in Figure 1 highlight some of the dark fibrillar material that straddles these large-scale polarity inversion lines (PILs); the polarity distribution of the line-of-sight photospheric field, smoothed to the spatial scale of the supergranulation, is displayed in Figure 1(f). Note that this dark canopy material is distinct from the arrowed filaments, which are closely aligned with the internal PIL of the active region.

Figure 2 shows a close-up of the northern edge of the active region canopy, as observed in Fe IX 17.1 nm at 17:01 and 23:01 UT on August 20. The corresponding line-of-sight magnetograms, smoothed to a resolution of $2''$ (to reduce the noise level) and saturated at ± 30 G, are displayed at the right. Arrows indicate the presumed local direction of the horizontal fibril fields, with the arrowheads pointing toward the negative-polarity footpoints. The outer boundary of the dark canopy coincides very roughly with a string of positive-polarity network elements extending from northeast to southwest across the field of view; inside this “front line,” negative-polarity flux spreading outward from the decaying active region dominates. Even here, however, small positive-polarity flux elements are almost everywhere present. Thus, it is often difficult to ascertain whether a given fibril structure is rooted in positive or negative polarity.

The boxed areas labeled “A” and “B” in Figure 2 enclose newly formed (or newly darkened) fibril structures located next to opposite-polarity flux elements in close contact, which in turn appear as compact 17.1 nm bright points. By constructing time-lapse movies at 30-min cadence,³ we have verified that these flux elements are in the process of converging and canceling. The box labeled “C” encloses a string of small emerging bipoles; note, however, that most of the mixed-polarity flux in these magnetograms represents preexisting network and intranetwork elements that are undergoing random encounters in the supergranular flow field, rather than ephemeral regions (for a discussion of network, intranetwork, and ephemeral region fields and their interactions, see Martin 1988).

During the first 3 weeks of 2010 August, a dark canopy that stretched across $\sim 180^\circ$ of longitude, extended from below the equator to above $L \sim +40^\circ$, and contained a number of new-cycle active regions, was observed rotating across the solar disk. The left column of

³Reduced-resolution HMI and AIA movies can be viewed at <http://sdo.gsfc.nasa.gov/data/aiahmi/browse.php>.

Figure 3 displays this giant northern-hemisphere canopy as it appeared on August 11 in an $H\alpha$ filtergram taken at the Big Bear Solar Observatory (BBSO), in a 17.1 nm image from AIA, and in an HMI magnetogram saturated at ± 30 G (after $2'' \times 2''$ smoothing) and at ± 0.1 G (after $60'' \times 60''$ smoothing). The right column of Figure 3 shows the same area one rotation later on September 8, after the active region fields have undergone further weakening and dispersal. It is evident that the 17.1 nm fibrils are now more concentrated around the large-scale polarity inversions, forming structures that more closely resemble PIL-aligned filaments. In particular, the northern section of the canopy has evolved into a U-shaped filament channel (see the boxed area) enclosing the sheared, negative-polarity remnant of the large active region on the southwest side of the canopy. Correspondingly, the $H\alpha$ image shows filament material extending along the northern edge of the canopy, which was not present on August 11.

Figure 4 focuses on the far western edge of the same northern-hemisphere canopy, as it appeared at 12:01 UT on August 8. The dark fibrils originating from the negative-polarity plage around the sunspot (located at the bottom left corner of the images) are seen to fan out more or less radially into the nearby network; the outer endpoints can be presumed to have positive polarity, even though they are sometimes located where both polarities are in close proximity or where the flux is very weak. Somewhat farther to the west, where the dominant polarity changes from negative to positive, the fibril structures become oriented more or less parallel to the large-scale PIL. Considering now the small active region on the right-hand side of these images, we observe a fountain pattern of dark fibrils that occupy a corridor of weak line-of-sight field and connect the negative-polarity plage to the positive-polarity background network lying to the west. Viewed from the positive-polarity side of the PIL, the field lines point to the right, consistent with the “dextral” handedness characterizing the majority of northern-hemisphere filaments (Martin et al. 1994; Martin 1998). The fibrils and “proto-filaments” surrounding the large active region on the left-hand side of the images likewise exhibit dextral handedness.

The sequence of 17.1 nm images and magnetograms in Figure 5 shows how the northern edge of the giant canopy evolves during August 10–13 (the field of view lies within the boxed area in Figures 3(a)–3(d)). Here, we see a collection of dark, featherlike structures lying between the predominantly positive-polarity area to the north and the sheared band of negative-polarity flux originating from the active region to the southwest. Early on August 10 (Figures 5(a) and 5(b)), the fibrils inside the white box are oriented almost perpendicular to the large-scale PIL, which is clearly defined by the line of strong negative-polarity network elements stretching from northeast to southwest. Over the next two days, the negative-polarity flux spreads northward into the positive-polarity background region, and the two polarities intermingle; at the same time, the fibrils begin to bend in the direction of the PIL.

In time-lapse movies, separate clumps of 17.1 nm fibrils oriented at different angles to each other are seen merging into longer structures with intermediate orientations (as in Figures 2 and 3 of Wang & Muglach 2007). Movies made from the HMI magnetograms show rapid flux cancellation occurring at the PIL, as well as rotational shearing, with the positive-polarity flux elements drifting eastward relative to the negative-polarity region to the south. By August 13, the fibrils have coalesced into long, filament-like structures that are more or less aligned with the PIL. It should be emphasized that the observed change in orientation of the fibrils relative to the PIL cannot be due to the photospheric differential rotation alone, which would cause a north–south aligned fibril with endpoints at latitudes 36° and 42° to tilt only $\sim 14^\circ$ over a 4-day period.

The characteristic height or vertical extent h_{171} of a 17.1 nm fibril above the photosphere can be estimated by comparing the corrugated texture of the limb in 17.1 nm with AIA images taken at 450.0 nm. From the fact that the fibril structures typically protrude $\sim 6''$ – $8''$ beyond the white-light limb, we deduce that $h_{171} \sim 4000$ – 6000 km, well above the nominal height of the chromospheric–coronal transition region.

3. Physical Interpretation

We proceed from the basic premise that the dark features seen in Fe IX 17.1 nm represent horizontal flux tubes that contain chromospheric material and connect photospheric flux elements of opposite polarity. (The cool material may consist of neutral hydrogen and helium which absorb the EUV radiation impinging from below: see, e.g., Chiuderi Drago et al. 2001; Rutten 2007.) Such horizontal fields form low-lying canopies that fan out from the edges of magnetic flux concentrations, whether they be active regions, sunspots, or network boundaries/vertices (Harvey 2005, 2006). In emerging active regions, the flux balloons outward in a dipole-like configuration and the surface-skimming field lines become connected to background network and intranetwork elements, forming a pattern of dark fibrils diverging from the area occupied by strong plage (as sketched in Figure 10 of Wang & Muglach 2007).

We expect the fibril pattern to continue to expand outward even after the active region has fully emerged, because of the diffusive effect of the nonsteady supergranular convection, which causes the plage to disintegrate and spread into the weaker-field background. The flux is swept to the boundaries of the randomly distributed supergranular cells, which have a characteristic diameter of $\sim 30,000$ km and lifetime of 1–2 days. As the cells decay and re-form at other locations, the fibril patterns continually change in response, in such a way that the fibrils remain centered above areas of relatively weak photospheric field, while their

endpoints remain anchored in network or intranetwork elements of opposite polarity. Flux cancellation will act to weaken the network fields, with the fibrils rooted in the canceling flux merging into longer structures. Other fibrils may split apart if the convective flows bring sufficiently strong network or intranetwork elements between their endpoints or if new bipoles emerge underneath them.

The canopy grows until the local rate of flux cancellation becomes so high that the diffusing active-region flux can no longer penetrate into the surrounding network. The outer boundary of the canopy thus stabilizes around a large-scale PIL separating the active region remnant from background field dominated by the opposite polarity. Continued flux cancellation around the PIL acts to submerge the transverse field component; as a result, the fibrils in this region become increasingly aligned with the PIL, and eventually coalesce into long filaments (see, e.g., van Ballegooijen & Martens 1989). This surviving axial field was generated in part by the photospheric differential rotation, which also acts to speed up the diffusive annihilation of flux at the PIL; in addition, it may contain a contribution arising from the intrinsic helicity of the original active region. However, shearing motions alone cannot account for changes in the orientation of the fibrils on timescales of a few days; flux cancellation is required to produce the observed rapid alignment with the PIL (cf. Wang & Muglach 2007).

An important observational result is that the dark 17.1 nm fibrils, once they have become detached via reconnection and diffusive transport from their active region source, tend to accumulate in areas of weak or mixed-polarity flux. This tendency is easily understood, given our assumption that fibrils are low-lying horizontal fields. Such field lines are more likely to reconnect with other low loops than with the high loops that are rooted inside strong unipolar flux concentrations (see Figure 6). Small, low-lying loops are in turn associated with mixed-polarity flux, whether in the form of canceling network elements, intranetwork fields, or small ephemeral regions. The net effect is to concentrate the fibrils around the large-scale background PILs surrounding the active region, where the bulk of the mixed-polarity flux is located. Systematic flux cancellation in this region then expedites the conversion of the fibrils into PIL-aligned filaments.

In his seminal studies of $H\alpha$ fine structure, Foukal (1971a, 1971b) came to the conclusion that $H\alpha$ fibrils cannot connect across supergranule cells, but must be open-ended absorbing features that bend upward and link to remote areas where the network has the opposite polarity. This conclusion was based on inspection of a then-available magnetogram showing that the opposite sides of a supergranule are usually of the same polarity. However, it has since become clear from higher-resolution observations that so-called unipolar regions contain large amounts of minority-polarity flux; indeed, Schrijver & Title (2003) assert that as

much as one-half of the strong network flux connects down into the immediately surrounding intranetwork areas. We also note that, because the magnetic network becomes increasingly fragmented toward the peripheries of active regions, horizontal field lines that are not “captured” by nearby loops are as likely to be channeled through gaps in the network as to be deflected sharply upward into the corona, as in Foukal’s picture.

High-cadence movies made from the full-resolution 17.1 nm images suggest that the fibril material streams continually from one footpoint to the other. These flows may be triggered by reconnection between the small loops and the fibril fields, generating chromospheric jets that inject new material into the fibrils. A similar process is thought to supply mass to H α and He II 30.4 nm filaments, where upflows and downflows of $\sim 5\text{--}70$ km s $^{-1}$ are observed (Zirker et al. 1998; Litvinenko & Martin 1999; Wang 1999; Kucera et al. 2003).

We have earlier remarked that areas of weak, “salt-and-pepper” fields far from active regions (such as that at the upper right corner of the images in Figure 1) are brighter than the canopy regions in Fe IX 17.1 nm, whereas the opposite is the case in higher-temperature coronal lines. The darkness of the 17.1 nm canopy is due to the presence of the organized, large-scale horizontal fields originating from the active region; in the quiet Sun, the fibrils are smaller and oriented more randomly, except around large-scale PILs, where systematic flux cancellation takes place. In contrast, the emission from coronal loops is correlated with their footpoint field strengths, so the quiet Sun generally appears darker than the areas immediately surrounding active regions when observed in lines such as Fe XII 19.3 nm and Fe XIV 21.1 nm.

4. Conclusions

We have used high-resolution Fe IX 17.1 nm images and longitudinal magnetograms from *SDO* to explore the relationship between the circumfacular areas or “dark canopies” surrounding active regions and the evolving photospheric field. Our main conclusions may be summarized as follows:

1. As has long been recognized, the canopies consist of dark fibril-like structures that appear as soon as the active regions emerge; the low-lying horizontal field lines balloon out over the surrounding area and reconnect with the background network to form a quasiradial or vortical pattern. The 17.1 nm fibrils overlie areas of relatively weak photospheric field.
2. The nonsteady supergranular convection causes the fibril fields to spread outward from the active region, with the outer boundary of the dark canopy stabilizing where the diffusing flux encounters a unipolar region of the opposite sign.

3. The 17.1 nm fibrils are often rooted in mixed-polarity regions, because of the tendency for the horizontal flux tubes to reconnect with small, low-lying loops.

4. As a result of this attraction toward mixed-polarity flux, the diffusing 17.1 nm fibrils gradually accumulate around large-scale PILs.

5. Systematic flux cancellation at the PIL removes the component of the field transverse to the PIL and progressively converts the fibrils into PIL-aligned structures.

6. In the absence of new flux emergence, active region canopies thus evolve toward a state where the dark material becomes concentrated around the surrounding background PILs, forming proto-filaments and filaments.

This study, like that of Wang & Muglach (2007) where $H\alpha$ observations were employed, points to the primary role of photospheric flux cancellation and fieldline reconnection in the evolution of fibrils into filaments. By making full use of the high temporal resolution of the *SDO* observations, which we have not properly exploited here, it should be possible to track the evolution of individual fibril structures, to characterize their mass flows, to pinpoint their footpoint locations, to clarify the relationship between fibrils and chromospheric jets, and to determine more precisely how flux cancellation leads to the coalescence of fibrils and their transformation into PIL-aligned filament channels and filaments.

We thank N. R. Sheeley, Jr., P. R. Young, and P. Foukal for stimulating discussions, and the referee for detailed and constructive criticism of an earlier version of the manuscript. The data employed here were provided courtesy of NASA/*SDO*, the AIA and HMI science teams, and BBSO/NJIT. This work was supported by NASA, NSF, and the Office of Naval Research.

REFERENCES

- Bumba, V., & Howard, R. 1965, *ApJ*, 141, 1492
- Cauzzi, G., et al. 2008, *A&A*, 480, 515
- Chiuderi Drago, F., Alissandrakis, C. E., Bastian, T., Bocchialini, K., & Harrison, R. A. 2001, *Solar Phys.*, 199, 115
- Feldman, U., Dammasch, I. E., & Wilhelm, K. 2000, *Space Sci. Rev.*, 93, 411
- Foukal, P. 1971a, *Sol. Phys.*, 19, 59
- Foukal, P. 1971b, *Sol. Phys.*, 20, 298
- Hale, G. E., & Ellerman, F. 1903, *Publ. Yerkes Obs.*, 3(1), 3
- Harvey, J. W. 2005, *EOS Trans. AGU*, 86(18), 490
- Harvey, J. W. 2006, in *Solar Polarization 4*, ed. R. Casini & B. W. Lites (ASP Conf. Ser. 358; San Francisco, CA: ASP), 419
- Howard, R., & Harvey, J. W. 1964, *ApJ*, 139, 1328
- Kucera, T. A., Tovar, M., & De Pontieu, B. 2003, *Sol. Phys.*, 212, 81
- Litvinenko, Y. E., & Martin, S. F. 1999, *Sol. Phys.*, 190, 45
- Martin, S. F. 1988, *Sol. Phys.*, 117, 243
- Martin, S. F. 1998, *Sol. Phys.*, 182, 107
- Martin, S. F., Bilimoria, R., & Tracadas, P. W. 1994, in *Solar Surface Magnetism*, ed. R. J. Rutten & C. J. Schrijver (NATO ASI Ser. C-433; Dordrecht: Kluwer), 303
- Moses, D., et al. 1997, *Sol. Phys.*, 175, 571
- Reardon, K. P., Uitenbroek, H., & Cauzzi, G. 2009, *A&A*, 500, 1239
- Rutten, R. J. 2007, in *The Physics of Chromospheric Plasmas*, ed. P. Heinzel, I. Dorotovič, & R. J. Rutten (ASP Conf. Ser. 368; San Francisco, CA: ASP), 27
- Schrijver, C. J., & Title, A. M. 2003, *ApJ*, 597, L165
- St. John, C. E. 1911, *ApJ*, 34, 57
- van Ballegooijen, A. A., & Martens, P. C. H. 1989, *ApJ*, 343, 971
- Wang, Y.-M. 1999, *ApJ*, 520, L71
- Wang, Y.-M. 2001, *ApJ*, 560, 456
- Wang, Y.-M., & Muglach, K. 2007, *ApJ*, 666, 1284
- Veeder, G. J., & Zirin, H. 1970, *Sol. Phys.*, 12, 391

Zirker, J. B., Engvold, O., & Martin, S. F. 1998, *Nature*, 396, 440

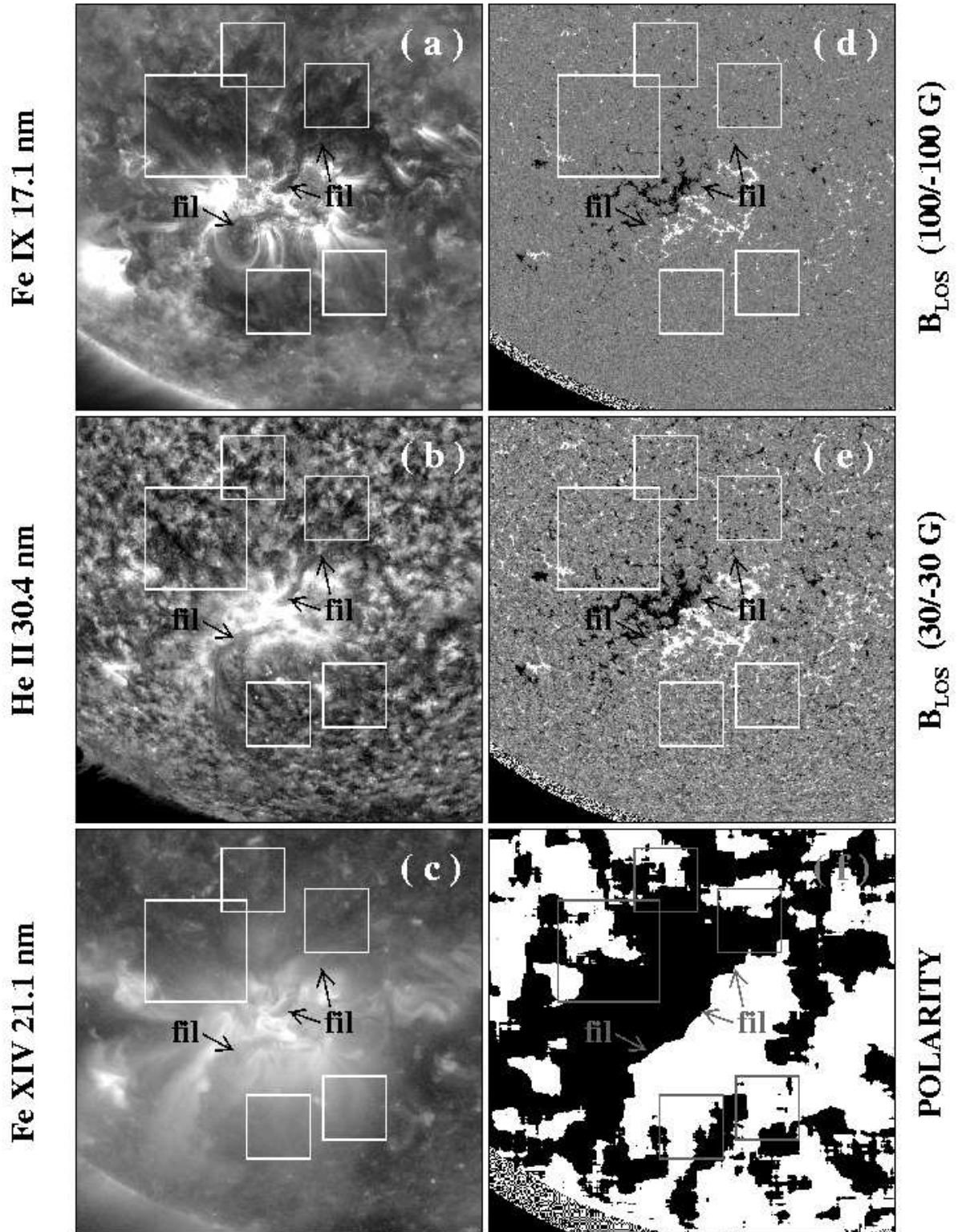


Fig. 1.— AIA and HMI images showing a “dark canopy” surrounding an active region in the southern hemisphere, 2010 August 20 at 23:01 UT. (a) Fe IX 17.1 nm. (b) He II 30.4 nm. (c) Fe XIV 21.1 nm. (d) Simultaneous line-of-sight magnetogram saturated at ± 100 G. (e) The same magnetogram saturated at ± 30 G after $2'' \times 2''$ smoothing. (f) Polarity distribution after smoothing the magnetogram with a $60'' \times 60''$ running window. Boxes highlight areas containing dark fibrillar material and relatively weak longitudinal field, where the spreading active-region flux encounters background network of the opposite polarity. Arrows point to a large filament aligned with the internal PIL of the active region.

2010 AUGUST 20

Fe IX 17.1 nm

B_{LOS} (30/-30 G)

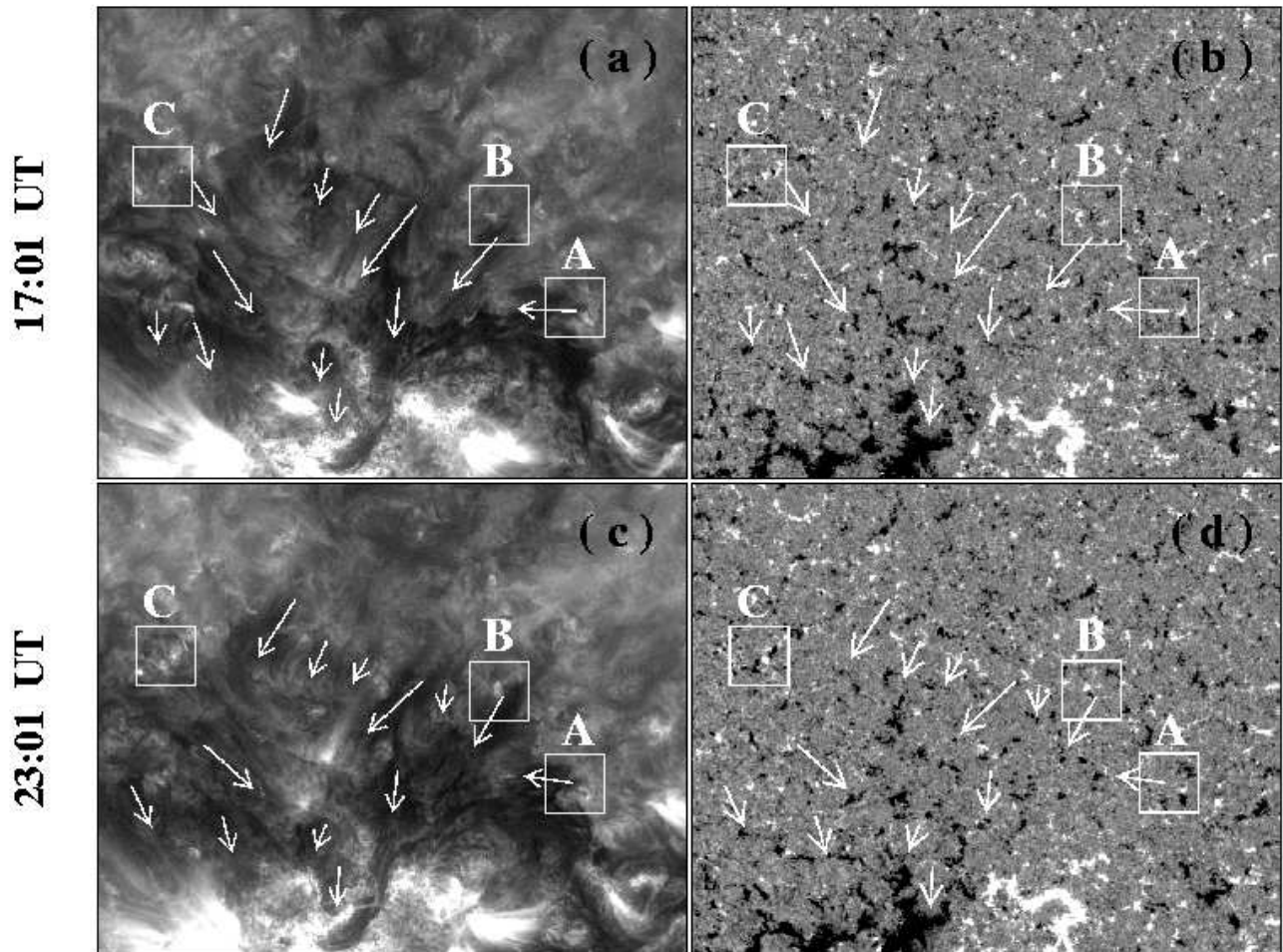


Fig. 2.— Close-up of the northern edge of the active region canopy in Figure 1. Field of view has dimensions $530'' \times 424''$; north is up and west is to the right. (a) Fe IX 17.1 nm image recorded at 17:01 UT on August 20. (b) Simultaneous line-of-sight magnetogram, smoothed to a resolution of $2''$ and saturated at ± 30 G. (c) Fe IX 17.1 nm image recorded at 23:01 UT on August 20. (d) Simultaneous line-of-sight magnetogram. Arrows indicate the presumed local direction of the horizontal fibril fields, with the arrowheads pointing toward the negative-polarity footpoints. Boxes labeled “A” and “B” highlight canceling magnetic flux elements; box “C” encloses newly emerged ephemeral regions.

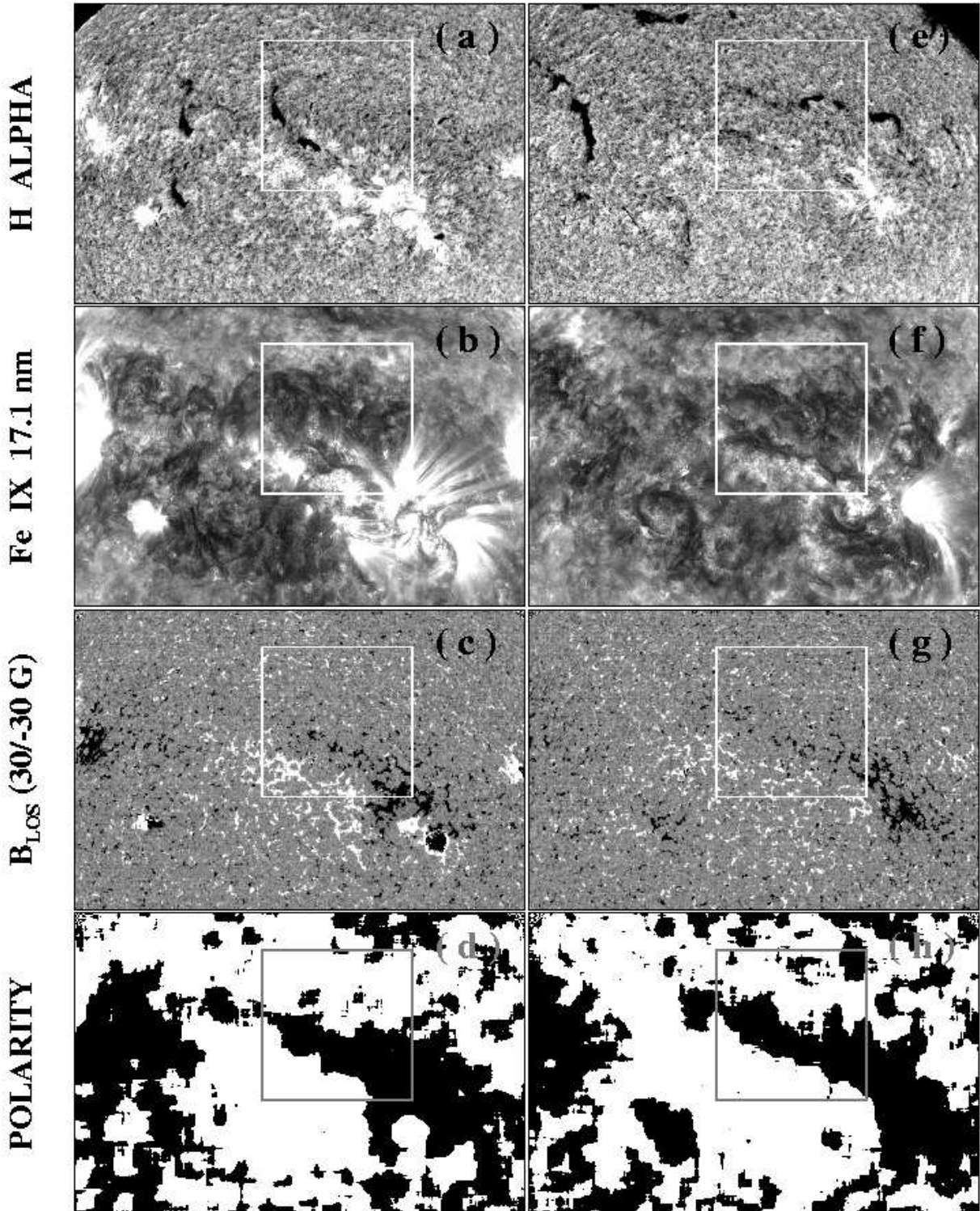


Fig. 3.— Giant northern-hemisphere canopy observed on 2010 August 11 (left panels) and one rotation later on September 8 (right panels). Field of view has dimensions $1268'' \times 845''$. (a) BBSO $H\alpha$ filtergram taken at 16:03 UT on August 11 (line-center observations with 0.025 nm bandpass). (b) AIA Fe IX 17.1 nm image recorded at 23:01 UT on August 11. (c) HMI longitudinal magnetogram (23:01 UT), saturated at ± 30 G after $2'' \times 2''$ smoothing. (d) Corresponding polarity distribution after $60'' \times 60''$ smoothing. (e) BBSO $H\alpha$ filtergram taken at 16:07 UT on September 8. (f) 17.1 nm image recorded at 05:01 UT on September 8. (g) longitudinal magnetogram recorded at 05:01 UT. (h) Corresponding polarity distribution. The boxed area evolves into a U-shaped filament channel as the active region fields decay

2010 AUGUST 8 (12:01)

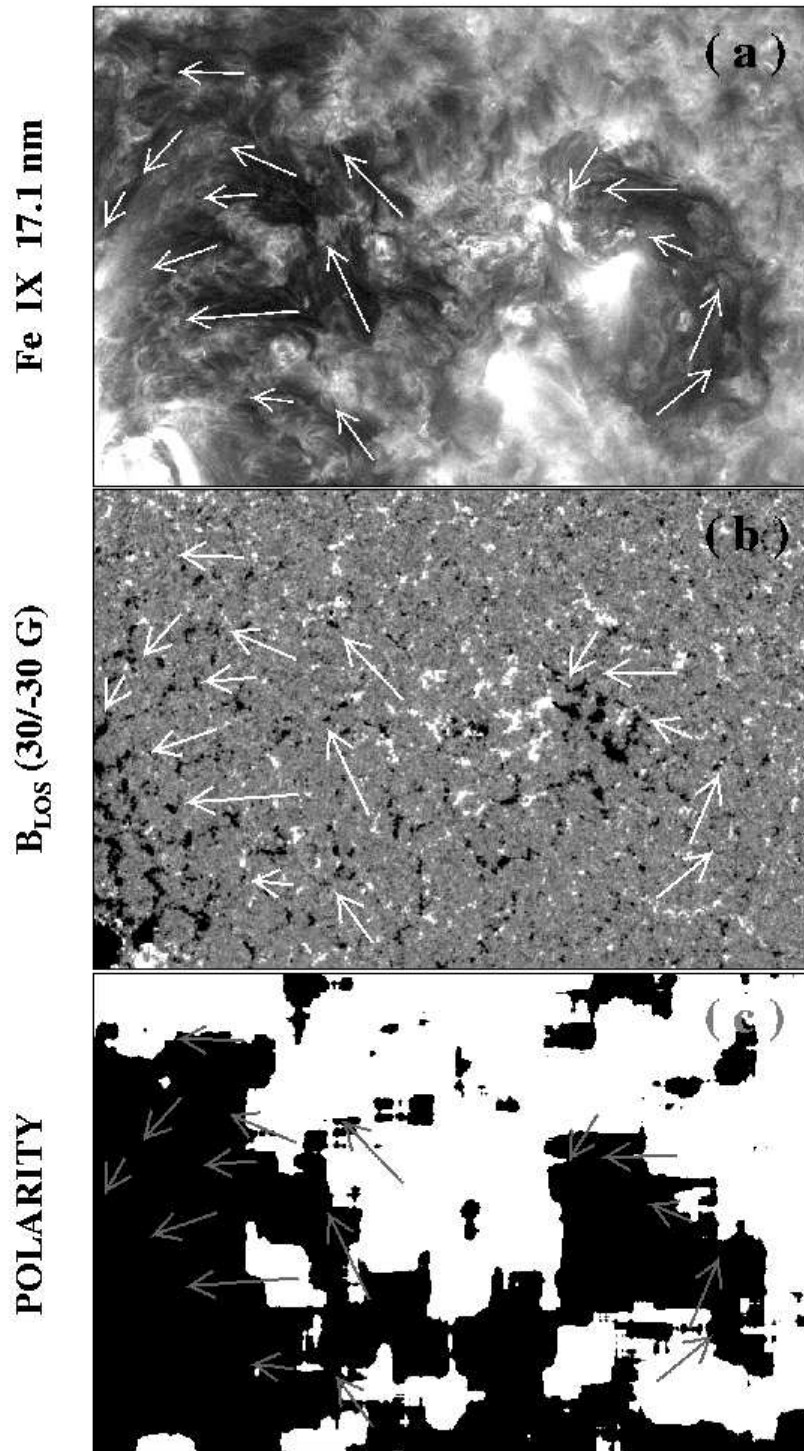


Fig. 4.— Far western edge of the giant northern-hemisphere canopy of Figure 3, as it appeared at 12:01 UT on August 8. Field of view has dimensions $634'' \times 423''$. (a) Fe IX 17.1 nm image. (b) Corresponding line-of-sight magnetogram, saturated at ± 30 G after $2'' \times 2''$ smoothing. (c) Polarity distribution after $60'' \times 60''$ smoothing. Arrows indicate the presumed local direction of the horizontal fibril fields.

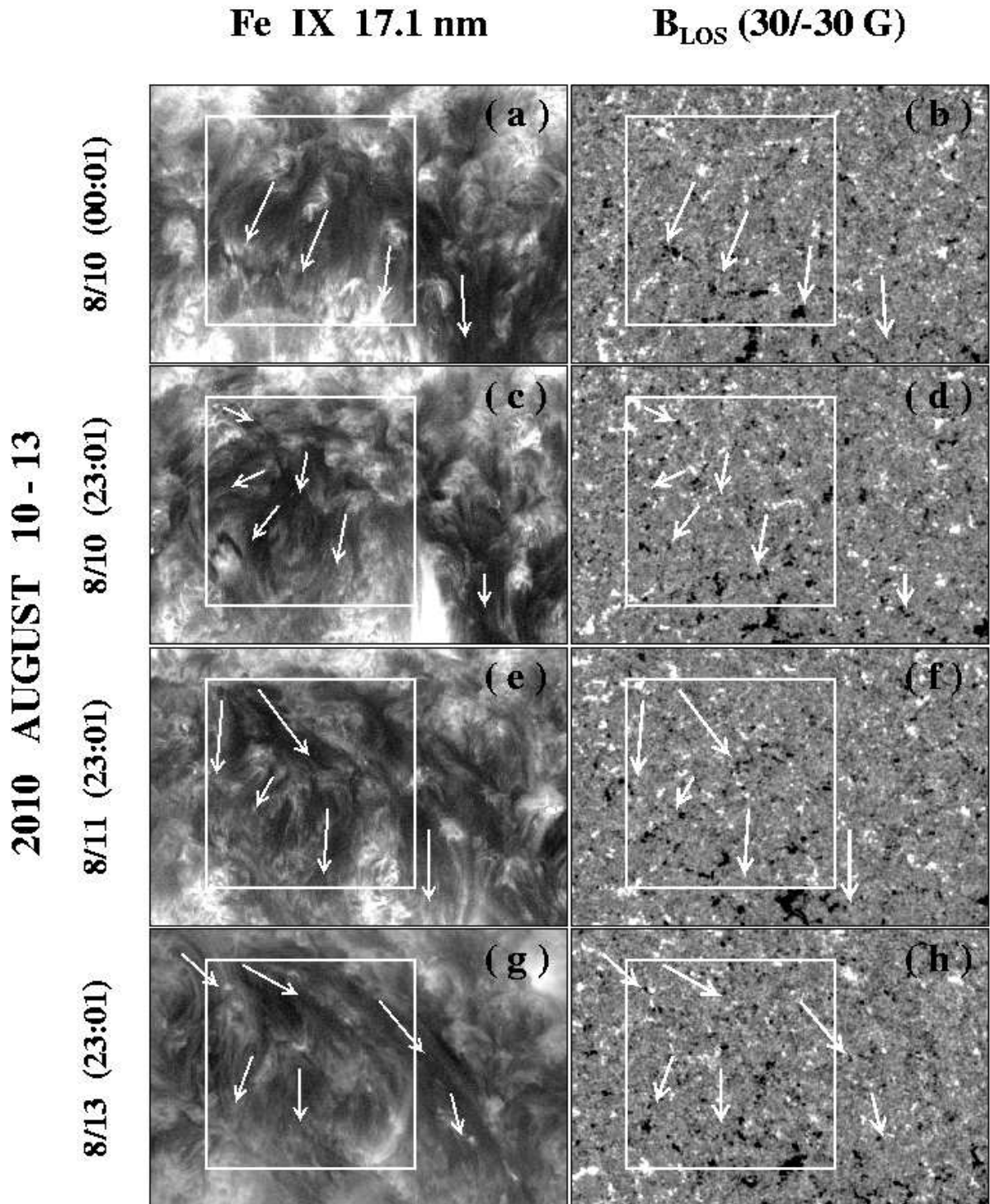


Fig. 5.— Sequence of 17.1 nm images (left) and corresponding longitudinal magnetograms (right), showing the evolution of the northern edge of the giant canopy of Figure 3 during August 10–13. Note the change in the orientation of the fibril structures inside the $158'' \times 158''$ boxed area (centered at $L \sim +37^\circ$), from nearly perpendicular to nearly parallel to the large-scale PIL, as the negative-polarity flux from the sheared active-region remnant diffuses into the positive-polarity background region to the north. Arrows indicate the presumed local direction of the horizontal fibril fields. The line-of-sight magnetograms are again saturated at ± 30 G after $2'' \times 2''$ smoothing.

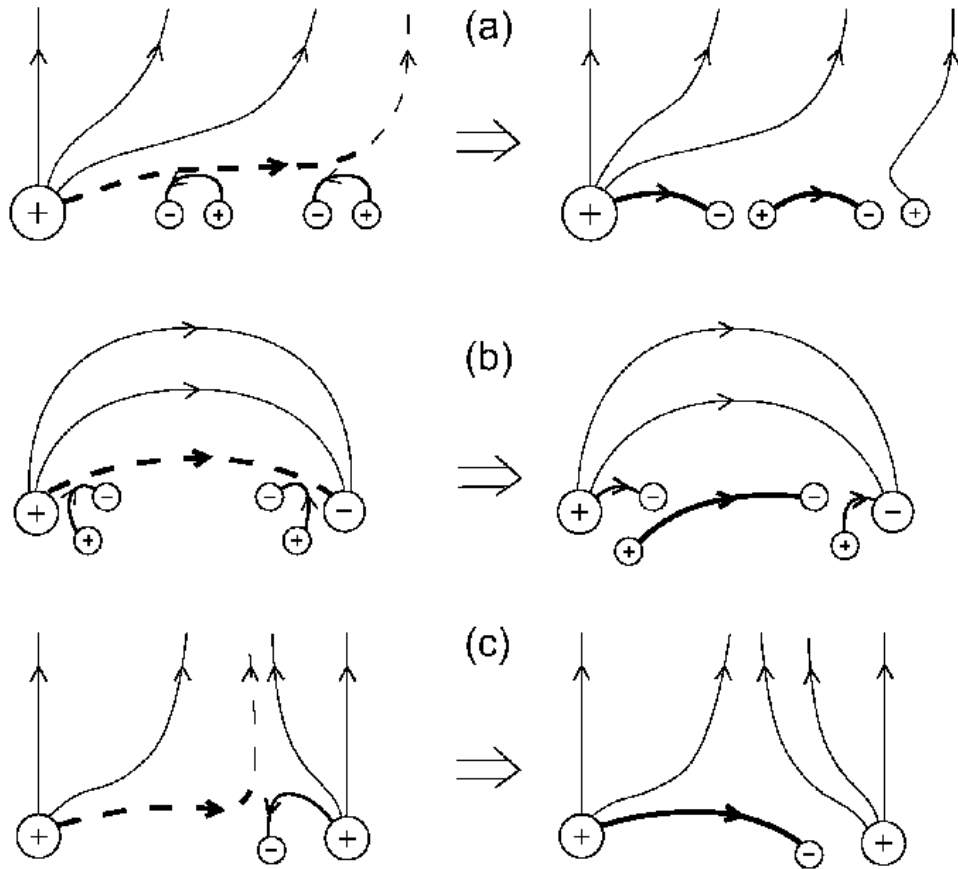


Fig. 6.— Low-lying, horizontal field lines have a natural tendency to become linked to weak, mixed-polarity network and intranetwork flux. (a) A long fibril (dashed) anchored in active region plage and extending out into the background network reconnects with a pair of small bipoles and splits into two pieces. (b) A fibril that initially links two strong, opposite-polarity network elements reconnects with the surrounding small bipoles and becomes rooted in weak, mixed-polarity flux. (c) Reconnection with small bipoles may also give rise to fibrils whose endpoints are located near strong network elements of the same polarity. In all of these cases, reconnection occurs at low heights and may trigger chromospheric jets that supply mass to the fibrils.